*Article*

# Numerical Investigation and Design Curves for Thinned Planar Antenna Arrays for 5G and 6G

Daniele Pinchera *[ID], Fulvio Schettino [ID], Mario Lucido [ID], Gaetano Chirico and Marco Donald Migliore [ID]

DIEI-Department of Electrical and Information Engineering "Maurizio Scarano", University of Cassino and S.L., via G.Di Biasio 43, 03043 Cassino, FR, Italy; schettino@unicas.it (F.S.); lucido@unicas.it (M.L.); gaetano.chirico@unicas.it (G.C.); mdmiglio@unicas.it (M.D.M.)
* Correspondence: pinchera@unicas.it

**Abstract:** We numerically investigate the relationship between the main parameters of thinned antenna arrays using a specifically designed evolutionary algorithm, the Multi-Objective Pareto Evolution for Thinning (MOPET). We provide some useful results that allow for the assessment of the achievable performance of antenna arrays and help researchers and practitioners design radar, 5G, and 6G systems. In particular, our approach allows us to quantify the advantage of thinned arrays with respect to traditional equispaced arrays (EA); as an example, using the same number of radiators, we can obtain the same directivity of an EA with a reduction in the side-lobe level (SLL) of more than 10dB, or increase the directivity of a couple of dB maintaining the same SLL of the EA, or get a combination of the two improvements. Moreover, the advantage of thinned architectures with respect to standard EA seems to improve with the increase in the dimension of the array.

**Keywords:** antenna arrays; thinned arrays; Pareto optimization; terrestrial communications; satellite communications; 5G; 6G

## 1. Introduction

Antenna arrays are considered one of the key technologies for 5G and 6G communication systems, and, undoubtedly, any forthcoming communication system will employ ever larger and sophisticated arrays to achieve higher and higher performance [1–3]. The reason behind this success is their capability to focus the electromagnetic field radiation in a specific direction, improving the received power and enabling sophisticated multiplexing communication schemes that allow the multiplication of the available system throughput by a factor that can be proportional to the number of radiators employed [4].

Unfortunately, even if the cost of high-frequency hardware has significantly been lowered in the last decades, the use of large antenna arrays for civil applications is still treated with caution because of the direct relationship between performance improvement and implementation and maintenance costs.

For this reason, the requirement for efficient antenna systems has accelerated the research of innovative, non-expensive architectures that could guarantee the requested specifications. The critical factor is the reduction in the number of transceivers [5] and the number of T/R modules that are effectively connected to one (or more) antennas, also referred to as "active elements".

One of these architectures is represented by clustered arrays [6–10], or arrays employing subarrays (Figure 1a). Using subarrays allows the exploitation of good directivity using a limited number of control points. However, this improvement is paid for by reducing the scanning capability, which for some applications may become limiting.

Another possibility is represented by the use of sparse [11–25], non-regular architectures (Figure 1b), since they can provide a good directivity, thanks to the improved overall antenna aperture, but, differently from clustered arrays, the performance of the radiated beams remain stable for significant scanning ranges [26].
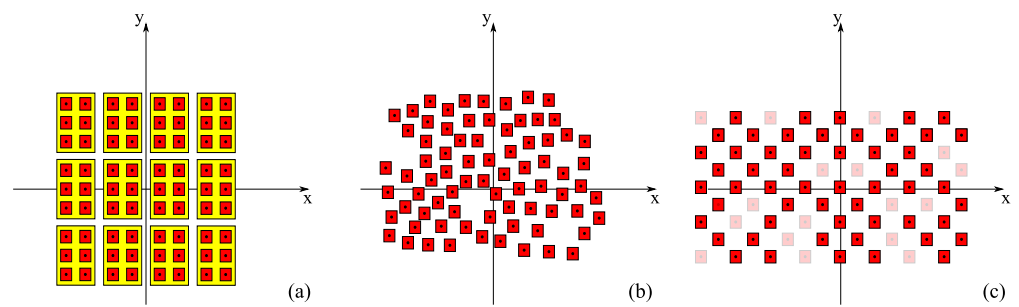
**Figure 1.** Scheme of some popular antenna array architectures. (**a**) Clustered/subarray architecture, where groups (marked in yellow) of radiators (marked in red) are fed by a single T/R module. (**b**) Sparse architectures, where the position of the radiators on the plane is freely selectable. (**c**) Thinned architectures, where the position of the radiators is selected starting from a regular grid.

Among the sparse antenna architectures, the thinned one is particularly appealing. In thinned architectures, the position of the radiators is obtained by selecting some elements from a regular grid (Figure 1c). This kind of array shows some advantages in the realization process, and they are also appealing for radar applications [27]; moreover, it could be possible to easily reconfigure the same antenna grid activating the elements that enable the wanted service, which is, in general, impossible to realize with sparse antennas.

It is well known that the synthesis of sparse antenna arrays, in its most general formulation, is challenging to solve; this difficulty is mainly due to the non-linear relationship between the radiated pattern and the positions of the radiators, but this problem is also true for thinned arrays for which the choice of the elements to turn on/off shares the limitations of NP-hard problems.

Because of these difficulties, thinned array synthesis has been largely investigated in the last decades; in particular, several deterministic techniques have been developed for their synthesis. Some examples are the quantization of a continuous aperture distribution [28], the use of difference sets [29–31], Minimax-inspired approaches [32], Fourier Transform-based methods [33–35], convex programming [36], the fractal approach [37], and the Quantum Fourier Transform method [38].

The use of evolutionary algorithms has also been demonstrated to be effective, and many approaches have been tested [39–48], also exploiting hybrid techniques [49–52] or machine learning methods [53].

Unfortunately, to the best knowledge of the authors, the problem of antenna array thinning has not been eviscerated satisfactorily from its multi-objective nature. Several parameters describe the quality of a radiation pattern (directivity, beamwidth, side-lobe level, number of employed elements, and so on), but only a few studies, like [54–59] have investigated these aspects properly.

In particular, no studies have deeply analyzed the performance realizable when a fixed number of active elements is employed. The focus on a specific number of elements is crucial since antenna engineers are often interested in evaluating the advantages of substituting a standard regular array with a different architecture, and one of the most effective ways to perform a comparison is considering a fixed cost, i.e., a fixed number of control points.

In this paper, we propose a methodology based on a specifically designed multi-objective optimization algorithm to face this problem, and several design curves will be also be provided to help the antenna engineers perform a preliminary dimensioning and benchmarking of the to-be-designed system.

The results that we will show will confirm that the use of thinned arrays may be advantageous with respect to traditional equispaced arrays (EA), providing an improvement of the directivity or a reduction in the SLL, or a combination of the two specifications.

Moreover, the thinned layouts synthesized with the presented approach could be used as an effective starting point for different kinds of layouts, like sparse arrays not based on regular grids.

The paper is organized in the following way. In Section 2, the antenna model will be discussed together with the calculation of pattern parameters. In Section 3, a novel algorithm, the Multi-Objective Pareto Evolution for Thinning (MOPET), will be presented and discussed. In Section 4, several results and design curves obtained with MOPET will be provided and discussed. Conclusions and future developments will follow.

## 2. Numerical Model

In this section, we will discuss the numerical model for antenna arrays employed in the paper. In particular, we will focus on synthesizing pencil beams with planar antenna arrays—linear arrays can be considered a sub-case. We will mainly evaluate the array factor (AF) [60] since it is equivalent to employing an isotropic element pattern, and this choice has the advantage of simplifying the reproducibility of the results provided.

Let $f$ be the working frequency, $\lambda$ the free-space wavelength, and $\beta = 2\pi/\lambda$ the free space wavenumber. With reference to Figure 2, where the position of the radiators on the $(x, y)$ plane is represented by ellipses of different colors according to their activation state, the position of the $N$ radiating elements of the array will be given by the vectors $\mathbf{x} = [x_1, x_2, \cdots, x_N]^T$ and $\mathbf{y} = [y_1, y_2, \cdots, y_N]^T$. For each element, the relative excitation will be stored in the vector $\mathbf{a} = [a_1, a_2, \cdots, a_N]^T$. The AF can then be calculated as follows:

$$AF(\theta, \phi) = \sum_{k=1}^{N} a_k e^{j\beta(x_k \sin\theta\cos\phi + y_k \sin\theta\sin\phi)} \tag{1}$$

where $(\theta, \phi)$ are the coordinates in the spherical coordinate system of Figure 2. Suppose the vector of the excitations contains only real positive numbers. In that case, the AF will show a pencil-like behavior, with a maximum in the $\theta = 0$ direction, also known as broadside direction.
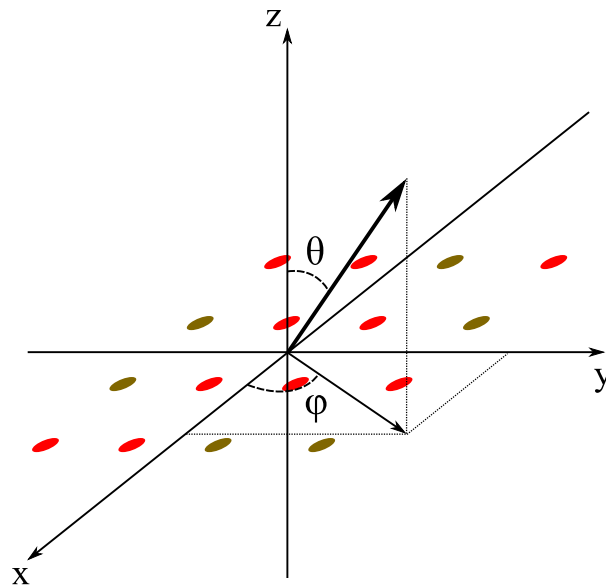


**Figure 2.** Scheme of the planar antenna array on the $(x, y)$ plane and of the coordinate systems employed. Ellipses with different colors represent the radiators according to their activation (red: active, brown: non-active).

As it is well-known, it is particularly convenient to introduce the two spatial variables $u = \sin\theta\cos\phi$ and $v = \sin\theta\sin\phi$, and to write the array factor as $AF(u,v)$; the directions $u^2 + v^2 \leq 1$ will represent the visible range of the array. This choice is particularly convenient when considering a linear-phase scanning of the array [60]; if the excitations are modified according to $a'_k = a_k e^{-j\beta(x_k u_s + y_k v_s)}$, the resulting AF will show its maximum in the direction $u_s, v_s$, since the pattern will be translated in the $(u,v)$ plane. It is then generally appropriate to calculate and optimize the AF for a range larger than the visible one to obtain an antenna array that can radiate a pattern that behaves well when scanned. In this paper, we will consider in most cases a portion of the $(u,v)$ plane such that $\sqrt{u^2 + v^2} \leq w_{MAX}$, where $w_{MAX} = 1 + \sin\theta_{MAX}$ takes into account the maximum scanning angle $\theta_{MAX}$ with respect to the broadside direction.

### 2.1. Main Pattern Parameters

The choice of the position and excitation of all the elements will influence the width of the radiated beam, the resulting directivity, and the amplitude/direction of secondary lobes.

One of the most common approaches regarding the main beam width is finding the angles for which the pattern is reduced by 3 dB with respect to its maximum. For planar arrays, in general, this corresponds to the identification of the shape of the footprint.

The directivity represents the capability of the array to focus energy in the main beam direction. For the broadside beam of an array of isotropic elements, it can be calculated as follows:

$$D = \frac{4\pi |AF(0,0)|^2}{\int_0^{2\pi}\int_0^{\pi} |AF(\theta,\phi)|\sin\theta d\theta d\phi} = \frac{\mathbf{a}^H \mathbf{a}}{\mathbf{a}^H \mathbf{S} \mathbf{a}} \tag{2}$$

where $*^H$ is the Hermitian operator, and $\mathbf{S}$ is a square matrix that depends on the type of employed elements; for isotropic elements, its entries are as follows:

$$s_{m,n} = \frac{\sin(\beta\rho_{m,n})}{\beta\rho_{m,n}} \tag{3}$$

with $\rho_{m,n} = \sqrt{(x_m - x_n)^2 + (y_m - y_n)^2}$ being the distance between two elements. The relationship (3) can be obtained from the well-known formula of the directivity for linear arrays [61], taking into account the symmetry of isotropic radiating pattern with respect to rotations of the coordinate system.

Finally, the side-lobe level is calculated as the ratio of the main beam AF with respect to the maximum in the other spatial directions:

$$SLL_{dB} = 20\log_{10}\left(\frac{AF(u,v)}{AF(0,0)}\right) \quad for \ (u,v) \ \in w_1^2 \leq u^2 + v^2 \leq w_{MAX}^2 \tag{4}$$

where $w_1$ is chosen to contain the main lobe on the $(u,v)$ plane. The verification of the SLL condition on a certain region of the $(u,v)$ plane allows us to verify that the side-lobe pattern requirements are verified for the wanted scanning angles; in (4), a circularly symmetric scanning capability with respect to the broadside direction is requested, but different choices could be made according to the overall system specifications.

### 2.2. An Observation on the Beamwidth

Some considerations on the relationship between beam width and directivity are now needed. From a practical point of view, the problem of the minimization of the beamwidth and the maximization of the directivity lead to very similar patterns, but while a directive pattern is always a pattern with a small beamwidth, the opposite may not be true because we can have a pattern with small beamwidth and a limited directivity, since some power can be wasted in non-focused directions, by side-lobes or grating lobes.

Moreover, the evaluation of the beamwidth is easily applicable with linear arrays or with factorable arrays (arrays in which the elements belong to a regular grid, and the

excitation of the $(m, n)$ element of the grid $a_{m,n} = b_m c_n$), since the resulting pattern will show an elliptical $-3$ dB footprint with the principal axes on the orthogonal $(u, v)$ directions, but may lead to ambiguities and difficulties in performing comparisons between different layouts when sparse or thinned architectures are employed. On the contrary, directivity is an unambiguously defined parameter.

For this reason, in the following, we will opt to focus on the optimization of directivity only and check the beam width only when specific comparisons will be needed.

### 2.3. Antenna Array Synthesis

The array synthesis problem can be formulated as finding the positions and excitations of the radiating elements of an antenna array to radiate a beam with the wanted directivity and an SLL below a prescribed threshold for the wanted scanning region.

The previously described procedure is inherently a multi-objective optimization problem that is, in general, more challenging to handle with respect to single-objective ones. In multi-objective problems, we have a set of competitive objectives that we would like to improve. Even if it is possible to use sophisticated weighting functions to reduce a multi-objective problem into a single-objective one [62–64], to face this kind of problem without a-priori choices, we should identify the so-called "Pareto boundary" (PB). This term refers to the set of optimal solutions where no solution can be improved in one objective without sacrificing performance in another.

## 3. Multi-Objective Pareto Evolution for Thinning

The identification of the PB can be achieved in several ways, but the most efficient one consists of using one of the algorithms that explicitly seek the PB [65]. In particular, some evolutionary algorithms have been developed to solve this task, and some popular ones are the SPEA [66] and NSGA-II [67]. These algorithms have already been fruitfully applied to the antenna array thinning problem [56,68], but in most cases, the number of radiating elements is considered one of the optimization parameters.

In this paper, we would like to focus on the achievable performance when a specific number of equal amplitude (or isophoric) radiators is employed. This approach is exciting from a practical point of view since it allows us to directly quantify the performance improvement when passing from a regular array architecture to a thinned array one.

To better solve this specific task, we have developed a novel evolutionary algorithm, MOPET, that takes inspiration from NSGA-II but is specifically tailored to the problem of finding the PB of thinned arrays.

### 3.1. Description of the Algorithm

The key point of MOPET is to achieve the evolution of the PB of the population of individuals; its main steps are described in the following:

1.  **Identify grid:** a grid of $M_{tot}$ antennas is defined, fixing its type (rectangular or triangular [69]), the number of rows $M_R$, the number of columns $M_C$, as well as the vertical spacing $d_v$ and horizontal spacing $d_h$.
2.  **Generate starting population:** A population of $N_{start}$ individuals is randomly generated. Each individual is represented by a binary string containing exactly $M_{on}$ ones so that the thinning rate is the same for each individual.
3.  **Remove duplicate members:** the population is checked for the presence of duplicated elements, and if found, they are removed.
4.  **Evaluate population:** the elements of the population are evaluated, and the PB is identified.
5.  **Weakly Dominated (WD) identification:** the elements not belonging to the PB are sorted according to the number of individuals that dominate them, then a set of the same size $N_{PB}$ as the PB is selected.

6.  **Grid centering of PB:** To reduce the issue of multiple equivalent solutions, the individuals belonging to the PB and WD are modified in order to have the "ones" centered on the grid. A graphical example of the centering of the excitations on the grid is provided in Figure 3.

7.  **Immigrant population (IP) generations:** a set of $N_{IP}$ novel random "immigrating population" individuals is generated, in order to avoid stagnation of the algorithm.

8.  **Crossover realization:** The individuals of PB, WD, and IP are randomly selected to generate $N_C$ Crossover Individuals (CI), using the Thinning-Rate-Preserving Crossover (TRPC). This function, described in Figure 4, allows us to perform a crossover between two binary genes that maintains the number of ones $M_{on}$ in the generated vectors.

9.  **Perform mutations:** The individuals of the PB and WD are subject to mutation, generating $N_{MI}$ Mutated Individuals (MI). For each MI, $M_{mut}$ elements of the group of "ones" of the individual are exchanged with $M_{mut}$ elements of the group of "zeros".

10. **Iteration:** a new population is formed joining the PB, WD, IP, CI and MI, and the algorithm returns to step 3, unless the maximum number of iterations $P_{max}$ is reached.
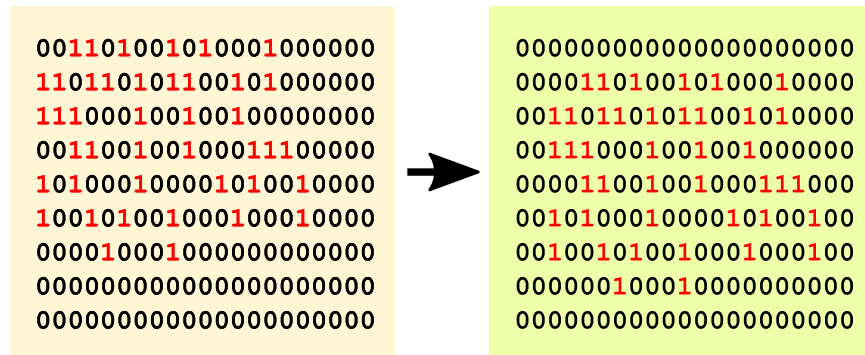


**Figure 3.** Graphical representation of the grid centering. On the left side, we can see the binary grid describing the excitation of the thinned array before the centering. In the right grid, the group of "1" of the binary grid representing the turned-on elements is shifted in order to have such elements centered on the overall grid. The red color of the "1" is used to emphasize the shift.
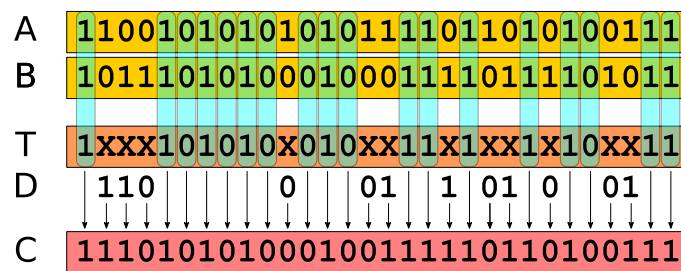


**Figure 4.** Graphical description of the Thinning-Rate-Preserving Crossover. A "XOR" operation is performed between two binary sequences (A,B) to identify their common bits (the position of the common bits is emphasized by means of cyan rectangles). A temporary trinary vector T is then generated (the "X" represents non-common bits of the two binary sequences to cross). Then, a random binary vector D, of the same length as the number of "X" of T, is generated; this sequence must have the same number of ones and zeros. Finally, the crossover vector C is obtained from T, substituting the "X" with the elements of D. Vertical arrows are used to show the origin of each bit.

The described algorithm has been implemented in a Matlab code and tested in various cases. Besides the fact that there are many steps involved in the iteration, these steps are sequential, and the overall implementation is relatively straightforward.

*3.2. A Deeper Insight on the Proposed Algorithm*

Some considerations on the algorithm are now in order.

- As with every evolutionary-based algorithm, MOPET is able to guarantee the achievement of the wanted solution asymptotically; several pattern evaluations are needed, but this request perfectly matches modern CPUs/GPUs, optimized for parallel processing. Moreover, as all the multi-objective optimization methods are based on the PB concept, the computational cost may not be convenient if we aim to calculate a single antenna layout; nevertheless, the final result of MOPET consists of multiple solutions, so the overall computational efficiency is often advantageous—it would take much more computation time to re-run a single objective optimization several times.

- The algorithm employs "elitism", so the PB from a previous generation is always passed to the successive one. This feature guarantees that the PB can only improve in the course of the algorithm without needing an external storage of solutions.

- The addition of WD individuals to the population that will be subject to crossover allows the preservation of the individuals close to the PB and whose descendants are likely to belong to the PB. The choice of having the WD of the same size as the PB has been verified to be a good compromise for the overall behavior.

- The size of the population should be proportional to the expected size of individuals of the PB, and two–three times the size of the expected PB seems to be fine; in this way, we guarantee that in the next population there will be a couple of newborns from each element of the PB and WD. Obviously, it is not possible to know in advance the size of the PB of a certain problem, and a bit of testing may be required when a completely novel problem is faced.

- Only the non-previously evaluated individuals are required to be calculated. This feature implies that there is no particular penalty for the algorithm if the size of the PB becomes very large.

- Differently from other algorithms like NSGA-II, there is no selection of the elements belonging to the PB according to a "crowding" principle.

- The duplicate element check and the use of an IP help prevent the algorithm from getting stuck around some local solutions. In the realized preliminary tests, not reported here for space constraints, we had found that the duplication of elements may lead to an oversearching in specific regions of the search space, slowing the convergence. Similarly, adding 5–10% of immigrants (with respect to the overall population) strongly reduces the need for multiple runs to achieve the desired results (all the results that will be shown are relative to single runs of the algorithm).

- The grid centering is particularly advantageous when a strong thinning is realized. Employing it, we are guaranteed that two individuals, like the ones depicted in Figure 3, that correspond to the same radiation pattern, are seen as two different individuals, resulting in a fake increase in the size of the PB.

- The use of mutations is beneficial in the latest stages of the optimization when the variation in a few elements can help to find nearby solutions. The use of about 10% of mutated individuals strongly improves the search effectiveness of the algorithm once the overall search space has been roughly explored.

- Regarding the termination of the optimization, in this paper, we have chosen to stop the execution after calculating a prescribed number of iterations; in this way, the overall calculation time is easily predictable. We have also tested as a termination criterion the verification of the stabilization of the size of the PB: when the size of the PB does not change after some tens of iterations, the algorithm has likely reached the optimal solutions, but this approach seems to increase the calculation time without a significant improvement in the overall quality of the identified PB.

## 4. Results and Discussion

In this section, we will present some results that validate the approach analyzed in the previous sections and provide some design curves that may help to design thinned and sparse array systems. All the results presented in this section are relative to simulations performed in Matlab running custom-implemented codes using an Intel 14900K-based office PC. The MOPET used to achieve the results in this section will employ the following parameters: $N_{start} = 1000$, $N_{MI} = 100$, $M_{mut} = 2$, $N_{IP} = 100$, $N_C = 800$, and $P_{max} = 30{,}000$. For the calculation of directivity, we have considered isotropic elements; the use of more directive radiators would slightly increase the directivity (of an amount approximately equal to the radiator's directivity), but the AF essentially dominates the pattern shape, so the proposed results can be used as a reference also when non-isotropic elements are employed.

### 4.1. A Preliminary Case Study

First, we will analyze a case study discussed in [34]. In particular, we will focus on a thinned antenna array of $M_{on} = 128$ elements able to radiate a pencil beam in the horizontal range $(-60°, +60°)$ and a vertical range $(-20°, +20°)$. To achieve this task, a rectangular grid of $M_c = 24 \times M_r = 12$ elements ($M_{tot} = 288$), with $d_v = d_h = \lambda/2$, has been selected. It is worth underlining that, from a combinatorial point of view, the overall number of different layouts of 128 elements from a grid of 288 is around $3.96 \times 10^{84}$; even if some of these layouts are equivalent (because of symmetries and translations), the overall number of possibilities is huge, and the synthesis problem cannot be solved by means of an exhaustive search.

In Figure 5, we can see the PB made of $N_{PB} = 298$ different arrays found with MOPET for the considered case. In the plot, it is also possible to see the comparison with the thinned solution presented in [34], as well as the comparison with the "standard" $\lambda/2$ equispaced rectangular array of 16 columns and 8 rows. It is clearly visible that both of these solutions are on the left side of the Pareto curve, meaning that the identified PB contains several solutions that dominate both the reference ones.
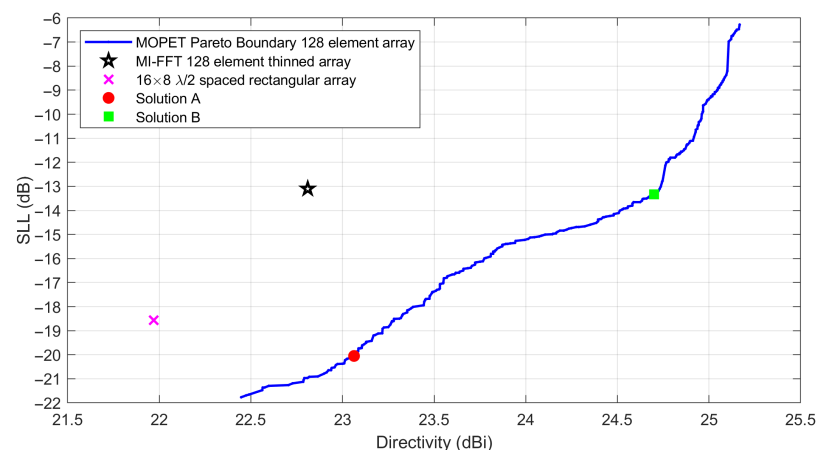


**Figure 5.** PB found with MOPET for the case of a rectangular antenna with 128 elements. Some reference solutions are compared to the Pareto curve.

To better understand this result, we will focus on analyzing a couple of solutions belonging to the identified PB. In Figure 6, we can see "Solution A". In this case, the synthesized array shows a broadside directivity of 23.06 dBi and an SLL lower than $-20.05$ dB for all the beams considered in the scanning range.

In Figure 7, we can see "Solution B". In this case, the synthesized array shows a broadside directivity of 24.70 dBi and an SLL lower than $-13.34$ dB for all beams considered in the scanning range.

It is worth noting that the choice of the simulation parameters has been made to improve the identification of the PB curve. In particular, running the algorithm for

$P_{max}$ = 30,000 iterations required about ten hours of calculation on an Intel 14900K-based office PC; this choice has been done to achieve a "smooth" and well-converged Pareto curve, but Pareto curves close to the final one were also achieved after just 3000 iterations. Finally, it should be mentioned that the antenna array synthesis task is an off-line task, and in most cases, the ability to explore the search space delivering quality solutions is much more important than pure speed. Moreover, the 10 h of calculation allowed us to generate not a single solution, like in other optimization algorithms, but different $N_{PB}$ = 298-optimal arrays, so the amount of time is acceptable.
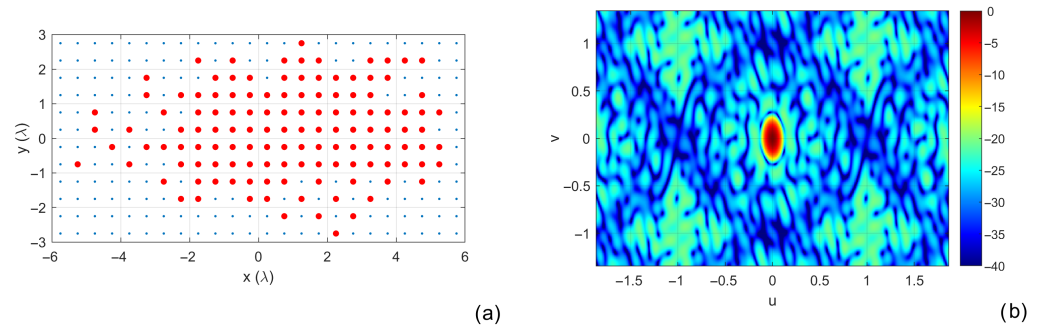


**Figure 6.** Analysis of Solution A from Figure 5. (**a**) Antenna layout, with the red circles representing the 128 used elements. (**b**) Normalized radiation pattern represented in the $(u, v)$ plane.
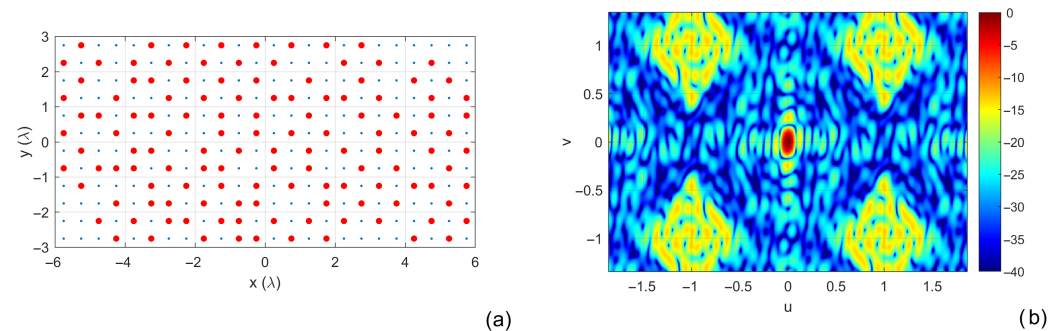


**Figure 7.** Analysis of Solution B from Figure 5. (**a**) Antenna layout, with the red circles representing the 128 used elements. (**b**) Normalized radiation pattern represented in the $(u, v)$ plane.

*4.2. A Second Case Study*

For the second case study, we will compare it with the result discussed in [59]. In this paper, the authors consider a rectangular grid of $M_c = 20 \times M_r = 10$ elements ($M_{tot} = 200$), with $d_v = d_h = \lambda/2$, and they perform a Pareto optimization with a multi-objective modified binary cat swarm optimization (MO-BCSO) algorithm to reduce the number of radiators; in particular, they show the result of a $M_{on} = 124$ elements array able to radiate a pencil beam with a SLL of $-21.2$ dB (no scanning of the beam is considered). Using the data relative to the selected 124 elements provided by the authors, we were able to calculate the directivity of the solution, which is equal to 23.07 dBi. Using MOPET, we selected the same grid and tried to calculate the PB of the synthesis problem.

In Figure 8, we can see the PB made of $N_{PB} = 124$ different arrays found with MOPET for the considered case after a couple of hours of calculations. In the plot, it is also possible to see the comparison with the thinned solution presented in [59], as well as the comparison with the "standard" $\lambda/2$ equispaced rectangular array of 16 columns and 8 rows (we have removed the 4 corner elements to obtain exactly 124 elements). Also in this case, we can see that both the reference solutions are on the left side of the Pareto curve, meaning that the identified PB contains several solutions that dominate both the reference ones.
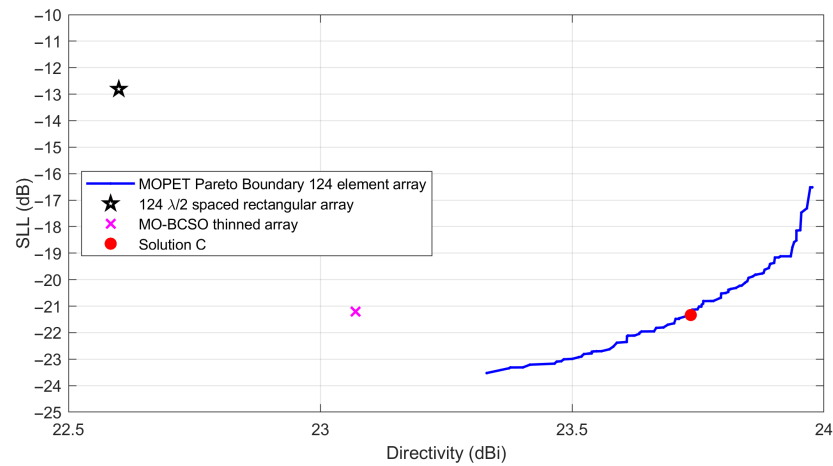
**Figure 8.** PB found with MOPET for the case of a rectangular antenna with 124 elements. Some reference solutions are compared to the Pareto curve.

We will examine a solution belonging to the identified PB. In Figure 9, we can see "Solution C". In this case, the synthesized array shows a broadside directivity of 23.67 dBi and an SLL lower than −21.25 dB.
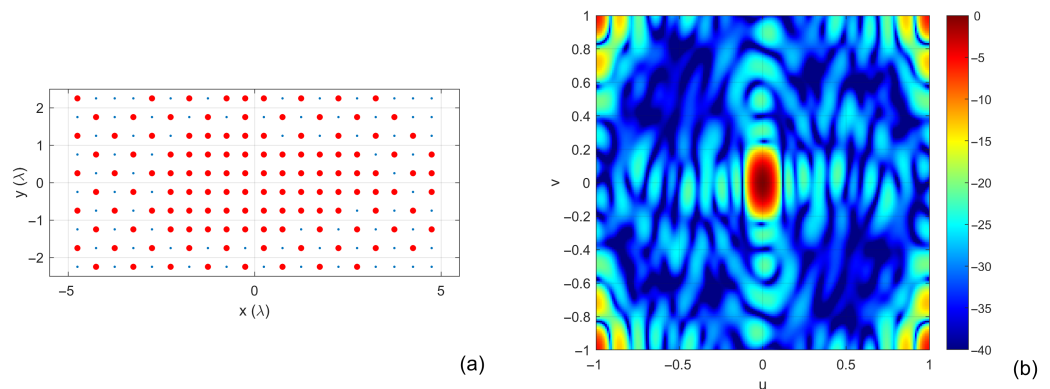


(a)



(b)

**Figure 9.** Analysis of Solution C from Figure 8. (**a**) Antenna layout, with the red circles representing the 124 used elements. (**b**) Normalized radiation pattern represented in the $(u, v)$ plane.

It is worth noting that the layout in Figure 9 does not show any symmetries; this result shows that the imposition of the symmetries over the x-axis and y-axis (a common assumption in array synthesis) may be beneficial from a computational point of view but may lead to non-optimal solutions.

### 4.3. Design Curves for Variable Grid and Number of Control Points

We will now investigate the synthesis of a pencil beam, considering two different cases: the radiation of a single broadside beam without scanning and the synthesis of a beam capable of scanning up to an angle of $60°$(deg), with respect to the broadside direction. The analysis will be then repeated for different numbers of active radiating elements ($M_{on} = \{64, 128, 256\}$). Moreover, we will analyze the effect of employing different types of grids (rectangular and triangular). The inter-element distance for the elements of the starting grid will be always $\lambda/2$.

In Figure 10, we can see the four PBs found with MOPET for the case of $M_{on} = 64$ compared to the reference case, with the $8 \times 8$ square planar array of the $\lambda/2$ isotropic elements. For the rectangular beam, we used a starting grid of $14 \times 14$ elements to be used in the thinning optimization, while for the triangular case, a grid of $14 \times 16$ elements was employed so that the overall starting layout was approximately square. It is clear that the requirement of a significant scanning range enormously lowers the achievable SLL for the

same level of directivity; moreover, the triangular lattice seems to perform better than the rectangular one: the two lattices are practically equivalent only in the case of the synthesis of a broadside-only beam with the lowest SLL.
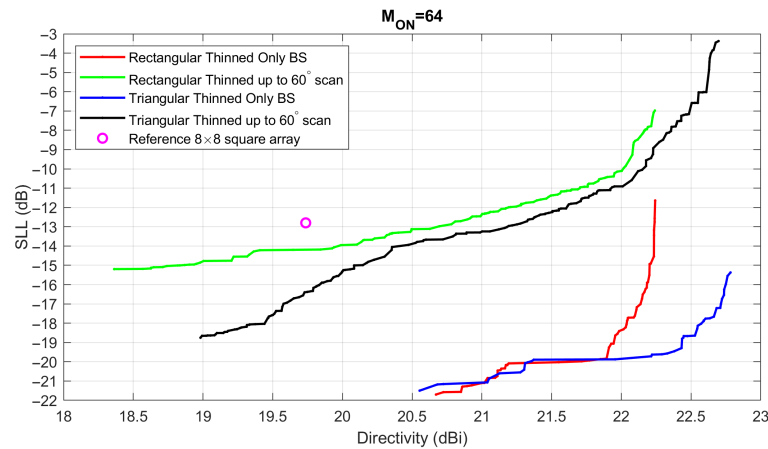


**Figure 10.** PBs for the square $M_{on} = 64$ case, compared to the reference solution.

In Figure 11, we can see the four PBs found with MOPET for the case of $M_{on} = 128$ compared to the reference case with the $11 \times 12$ "almost square" planar array of the $\lambda/2$ isotropic elements (the four corner elements of the regular grid have been removed to obtain exactly 128 elements). For the rectangular beam, we used a search grid of $20 \times 20$ elements, while for the triangular case, a search grid of $20 \times 24$ elements was employed so that the overall starting layout was approximately square. Again, we can see that the requirement of a significant scanning range strongly lowers the achievable SLL for the same level of directivity; in this case, the triangular lattice seems to perform better than the rectangular one only in the "broadside only" case; when considering a significant scanning, the triangular lattice is superior for the higher directivity layouts, while the rectangular lattice provides the lowest SLL.
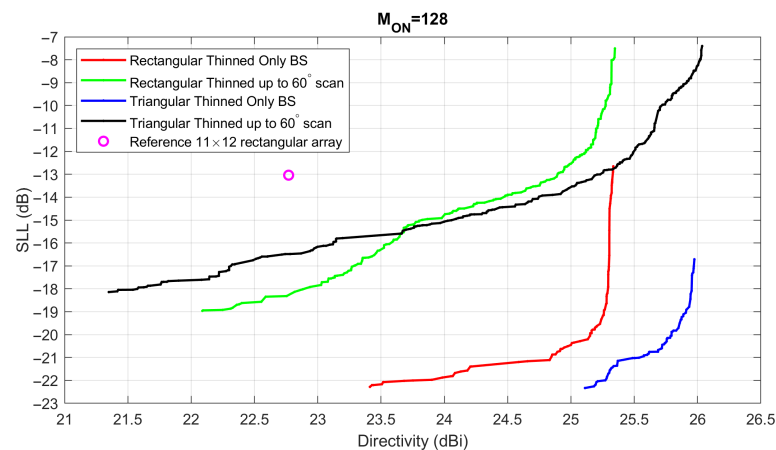


**Figure 11.** PBs for the square $M_{on} = 128$ case, compared to the reference solution.

In Figure 12, we can see the four PBs found with MOPET for the case of $M_{on} = 256$ compared to the reference case with the $16 \times 16$ square planar array of the $\lambda/2$ isotropic elements. For the rectangular beam, we used a search grid of $27 \times 27$ elements, while for the triangular case, a search grid of $27 \times 31$ elements was employed so that the overall starting layout was approximately square. Also, in this case, the request of a significant scanning range lowers the achievable SLL for the same level of directivity. As happened for the $M_{on} = 128$ elements, the triangular lattice seems to perform better than the rectangular one only in the "broadside only" cases, and in the scanning cases, the triangular lattice seems

to be superior for the higher directivity layouts, while the rectangular lattice provides the lowest SLL.
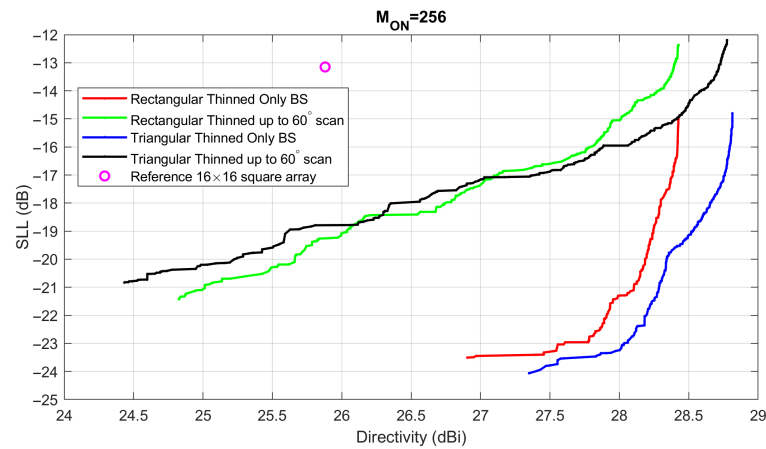


**Figure 12.** PBs for the square $M_{on} = 256$ case, compared to the reference solution.

From the results of Figures 10–12, it seems that the advantage of the thinned arrays with respect to the reference solutions increases when considering a greater number of elements: the more active elements, the more the thinned solution becomes advantageous. To better emphasize the overall behavior of the thinned solutions with a variable number of elements, in Figures 13 and 14, we have compared the results achieved for the broadside only cases and large scanning cases.
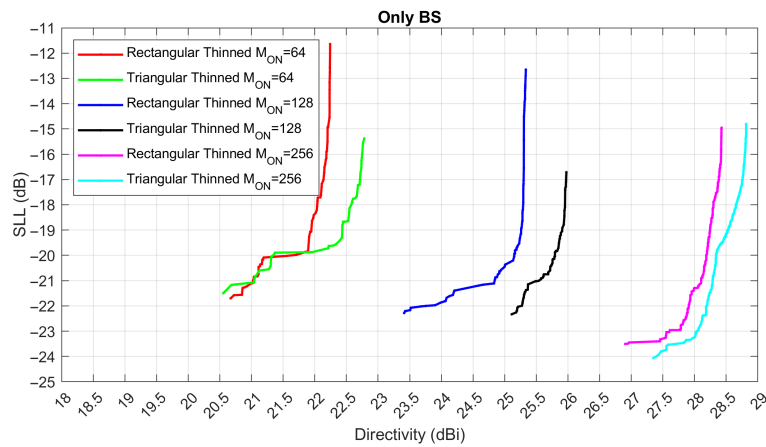


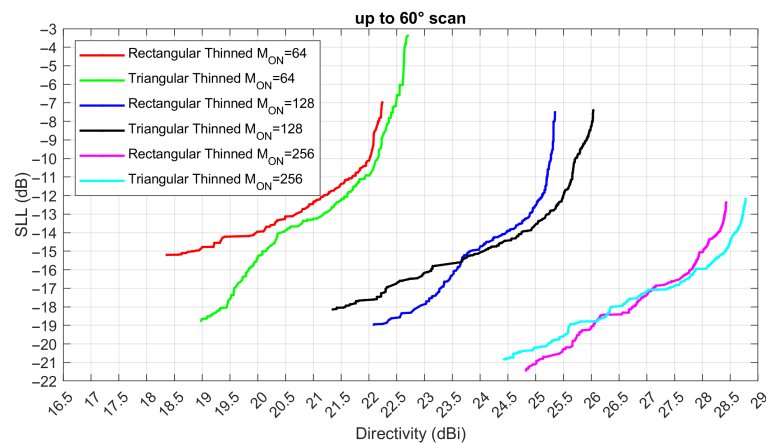**Figure 13.** PB curves for the $M_{on} = \{64, 128, 256\}$ broadside beam-only cases.



**Figure 14.** PB curves for the $M_{on} = \{64, 128, 256\}$ large scanning cases.

### 4.4. Very Large Planar Array Synthesis

As a last example, we will consider the synthesis of a very large planar array of $M_{on} = 1024$ elements able to radiate a pencil beam for any scanning angle within $\theta_{MAX} = 45°$, specifically focusing on achieving low side-lobe levels. According to the results of the previous subsection, we have selected a rectangular grid of $M_c = 45 \times M_r = 45$ elements ($M_{tot} = 2025$), with $d_v = d_h = \lambda/2$.

In Figure 15, we can see the PB made of $N_{PB} = 838$ different arrays found with MOPET for the considered case. In the plot, it is also possible to see the comparison with the "standard" $\lambda/2$ equispaced rectangular array of 32 columns and 32 rows. It is can be seen that a large portion of the solutions belonging to the PB dominate the reference equispaced array.
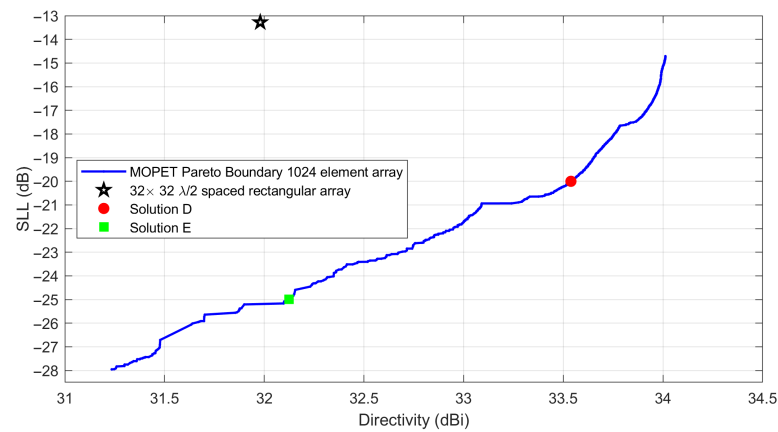


**Figure 15.** PB found with MOPET for the case of a rectangular antenna with 1024 elements. Some reference solutions are compared to the Pareto curve.

We will analyze some solutions to the identified PB to better understand this result. In Figure 16, we can see "Solution D". In this case, the synthesized array shows a broadside directivity of 33.54 dBi and an SLL lower than −20.00 dB for all beams considered in the scanning range. In Figure 17, we can see "Solution E". In this case, the synthesized array shows a broadside directivity of 32.13 dBi and an SLL lower than −25.00 dB for all beams considered in the scanning range. Both the results in Figures 16 and 17 show that the advantage of thinned arrays with respect to equispaced arrays is increased when lots of radiators are employed.
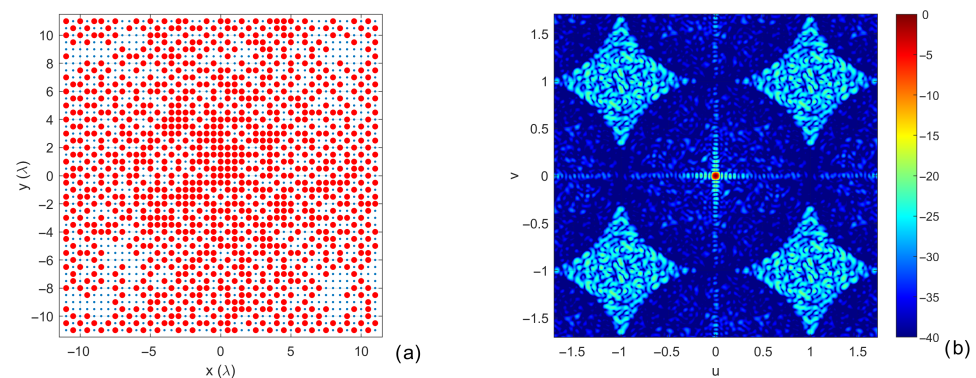


**Figure 16.** Analysis of Solution D from Figure 15. (**a**) Antenna layout, with the red circles representing the 1024 used elements. (**b**) Normalized radiation pattern represented in the $(u, v)$ plane.

**Figure 17.** Analysis of Solution E from Figure 15. (**a**) Antenna layout, with the red circles representing the 1024 used elements. (**b**) Normalized radiation pattern represented in the $(u, v)$ plane.
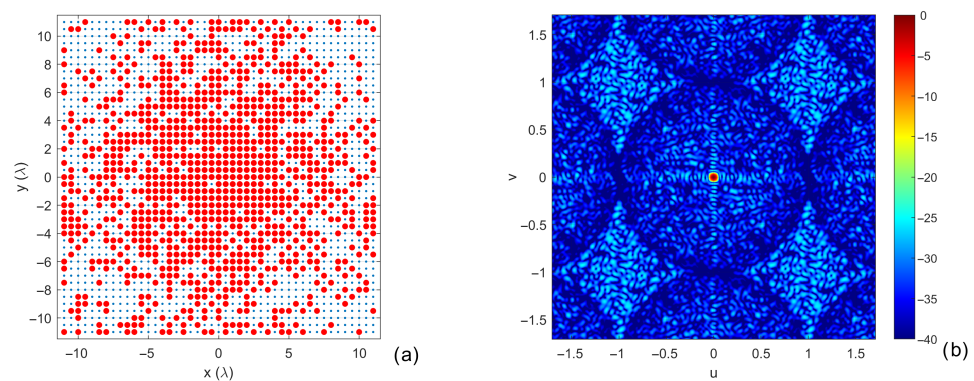
## 5. Conclusions

In this paper, we have investigated the thinned antenna array synthesis problem from a multi-objective perspective. In particular, a novel multi-objective evolutionary algorithm has been developed to achieve trustable results and investigate the specific case of fixed rate thinning. This algorithm, called MOPET, allows one to obtain the PB curves in a relatively limited time, and hundreds of different solutions—yet optimal from a Pareto perspective—can be achieved in a single run.

The choice of employing the same number of radiators, which represent the main source of the cost of active arrays, allows us to compare different architectures considering similar manufacturing costs.

Using the introduced method, we first analyzed a case study, confirming the effectiveness of the MOPET in achieving good solutions; after validating the approach, several optimizations employing rectangular and triangular lattices were tested. The achieved curves can be used "as is" to compare the results obtained from other synthesis methods or to achieve a rough benchmark of other arrays, but allow us to obtain some general design rules.

First, when limited scanning is required, the triangular lattice seems to be in general superior with respect to the rectangular one; when a large scanning is required, the rectangular array is instead superior when the lowest SLL is required, while the triangular lattice allows achieving slightly larger gains.

Moreover, the results show that non-regular architectures become more and more beneficial, both in directivity and side-lobe level, when many radiators are employed. To verify this hypothesis, we have investigated the case of a very large planar array of 1024 active elements, exploiting the considerations of the previous tests.

All the results shown confirm that the use of thinned arrays can be particularly advantageous with respect to traditional equispaced arrays. We can obtain the same directivity of an EA with a reduction in the side-lobe level (SLL) of more than 10 dB, or we can increase the directivity by up to a couple of dBs, maintaining the same SLL of the EA. The Pareto fronts identified clearly show that we can achieve the desired combination of the two improvements according to the specific synthesis requirement. Finally, as the 1024 active element example has demonstrated, the advantage of thinned architectures with respect to standard EA seems to improve with the increase in the dimension of the array.

It is worth recalling that the achieved results have been obtained for the case of isophoric arrays, so no amplitude control of the excitations has been considered. Furthermore, the thinned solutions achieved can be used as a starting point for other optimization algorithms that may move the radiators out of the positions of the lattice to achieve a better directivity and/or a lower SLL.

As a future development of the present research, we are currently working on using the MOPET also for the optimization of flexible or reconfigurable arrays [70–72]; we are

also investigating the possibility to use deep learning methods to improve the synthesis procedure and achieve quicker convergence.

## References

1. Guo, Y.J.; Ziolkowski, R.W. *Advanced Antenna Array Engineering for 6G and Beyond Wireless Communications*; John Wiley & Sons: Hoboken, NJ, USA, 2021.
2. Xiao, Z.; Han, Z.; Nallanathan, A.; Dobre, O.A.; Clerckx, B.; Choi, J.; He, C.; Tong, W. Antenna array enabled space/air/ground communications and networking for 6G. *IEEE J. Sel. Areas Commun.* **2022**, *40*, 2773–2804. [CrossRef]
3. Pinchera, D.; Migliore, M.D.; Schettino, F. Optimizing antenna arrays for spatial multiplexing: Towards 6G systems. *IEEE Access* **2021**, *9*, 53276–53291. [CrossRef]
4. Nam, J.; Ahn, J.Y.; Adhikary, A.; Caire, G. Joint spatial division and multiplexing: Realizing massive MIMO gains with limited channel state information. In Proceedings of the 2012 46th Annual Conference on Information Sciences and Systems (CISS), Princeton, NJ, USA, 21–23 March 2012; IEEE: Piscataway, NK, USA, 2012; pp. 1–6.
5. Toso, G.; Mailloux, R. Guest editorial for the special issue on innovative phased array antennas based on non-regular lattices and overlapped subarrays. *IEEE Trans. Antennas Propag.* **2014**, *62*, 1546–1548.
6. Spence, T.G.; Werner, D.H. Design of broadband planar arrays based on the optimization of aperiodic tilings. *IEEE Trans. Antennas Propag.* **2008**, *56*, 76–86. [CrossRef]
7. Bucci, O.M.; Pinchera, D. A Generalized Hybrid Approach for the Synthesis of Uniform Amplitude Pencil Beam Ring-Arrays. *IEEE Trans. Antennas Propag.* **2012**, *60*, 174–183. [CrossRef]
8. Rocca, P.; D'Urso, M.; Poli, L. Advanced strategy for large antenna array design with subarray-only amplitude and phase control. *IEEE Antennas Wirel. Propag. Lett.* **2014**, *13*, 91–94. [CrossRef]
9. Rocca, P.; Anselmi, N.; Polo, A.; Massa, A. Modular design of hexagonal phased arrays through diamond tiles. *IEEE Trans. Antennas Propag.* **2020**, *68*, 3598–3612. [CrossRef]
10. Akbar, F.S.; Ligthart, L.P.; Hendrantoro, G. A toolbox of subarrays for optimizing wide-angular scanning arrays using trade-offs between scan loss and side lobe level. *IEEE Access* **2021**, *9*, 16337–16359. [CrossRef]
11. Bucci, O.M.; Isernia, T.; Perna, S.; Pinchera, D. Isophoric sparse arrays ensuring global coverage in satellite communications. *IEEE Trans. Antennas Propag.* **2013**, *62*, 1607–1618. [CrossRef]
12. Chen, K.; Chen, H.; Wang, L.; Wu, H. Modified real GA for the synthesis of sparse planar circular arrays. *IEEE Antennas Wirel. Propag. Lett.* **2015**, *15*, 274–277. [CrossRef]
13. Salas-Sánchez, A.; Fondevila-Gomez, J.; Rodriguez-Gonzalez, J.; Ares-Pena, F. Parametric synthesis of well-scanning isophoric pencil beams. *IEEE Trans. Antennas Propag.* **2017**, *65*, 1422–1427. [CrossRef]
14. Pinchera, D.; Migliore, M.D.; Schettino, F.; Lucido, M.; Panariello, G. An effective compressed-sensing inspired deterministic algorithm for sparse array synthesis. *IEEE Trans. Antennas Propag.* **2017**, *66*, 149–159. [CrossRef]
15. Yan, C.; Yang, P.; Xing, Z.; Huang, S.Y. Synthesis of planar sparse arrays with minimum spacing constraint. *IEEE Antennas Wirel. Propag. Lett.* **2018**, *17*, 1095–1098. [CrossRef]
16. Pinchera, D.; Migliore, M.D.; Panariello, G. Synthesis of large sparse arrays using IDEA (inflating-deflating exploration algorithm). *IEEE Trans. Antennas Propag.* **2018**, *66*, 4658–4668. [CrossRef]
17. Wang, R.Q.; Jiao, Y.C. Synthesis of wideband rotationally symmetric sparse circular arrays with multiple constraints. *IEEE Antennas Wirel. Propag. Lett.* **2019**, *18*, 821–825. [CrossRef]
18. Gu, P.; Wang, G.; Fan, Z.; Chen, R. An efficient approach for the synthesis of large sparse planar array. *IEEE Trans. Antennas Propag.* **2019**, *67*, 7320–7330. [CrossRef]

19. Pinchera, D.; Migliore, M.D.; Lucido, M.; Schettino, F.; Panariello, G. Efficient large sparse arrays synthesis by means of smooth re-weighted l1 minimization. *Electronics* **2019**, *8*, 83. [CrossRef]

20. Zhao, D.; Wei, Y.; Miao, J. Adaptive gradient search for synthesis of planar array with arbitrary aperture shape. In Proceedings of the 2019 IEEE International Symposium on Phased Array System & Technology (PAST), Waltham, MA, USA, 11–14 October 2022; IEEE: Piscataway, NK, USA, 2019; pp. 1–5.

21. Miao, Y.; Liu, F.; Lu, J.; Li, K. Synthesis of unequally spaced arrays with uniform excitation via iterative second-order cone programming. *IEEE Trans. Antennas Propag.* **2020**, *68*, 6013–6021. [CrossRef]

22. Cui, C.; Li, W.T.; Ye, X.T.; Rocca, P.; Hei, Y.Q.; Shi, X.W. An effective artificial neural network-based method for linear array beampattern synthesis. *IEEE Trans. Antennas Propag.* **2021**, *69*, 6431–6443. [CrossRef]

23. Pinchera, D.; Migliore, M.D.; Panariello, G. Isophoric inflating deflating exploration algorithm (I-IDEA) for equal-amplitude aperiodic arrays. *IEEE Trans. Antennas Propag.* **2022**, *70*, 10405–10416. [CrossRef]

24. Miao, K.; Zhang, Y.; Wang, S.; Yao, C.; Zhao, G.; Sun, H. Synthesis of Sparse Planar Antenna Arrays Using A Matrix Constraints Method. *IEEE Trans. Antennas Propag.* **2024**, *72*, 4618–4623. [CrossRef]

25. Zeng, Y.; Ding, X.; Shao, W. Perturbation Theory-Based Method for Initial Arrangement of Large-Spacing Aperiodic Scanning Arrays. *IEEE Trans. Antennas Propag.* **2024**, *72*, 2837–2842. [CrossRef]

26. Buonanno, G.; Costanzo, S.; Solimene, R. Broadband statistically designed thinned-binned array antennas. *IEEE Trans. Antennas Propag.* **2023**, *71*, 2454–2466. [CrossRef]

27. Zhang, Z.; Schalch, J.S.; Yin, Y.; Rebeiz, G.M. Thinned Randomized 27–29 GHz TX and RX Arrays With Low Sidelobe Levels for Radars and 5G Communications. *IEEE Trans. Microw. Theory Tech.* **2023**, *72*, 1953–1963. [CrossRef]

28. Numazaki, T.; Mano, S.; Katagi, T.; Mizusawa, M. An improved thinning method for density tapering of planar array antennas. *IEEE Trans. Antennas Propag.* **1987**, *35*, 1066–1070. [CrossRef]

29. Leeper, D.G. Isophoric arrays-massively thinned phased arrays with well-controlled sidelobes. *IEEE Trans. Antennas Propag.* **1999**, *47*, 1825–1835. [CrossRef]

30. Oliveri, G.; Manica, L.; Massa, A. ADS-based guidelines for thinned planar arrays. *IEEE Trans. Antennas Propag.* **2010**, *58*, 1935–1948. [CrossRef]

31. Oliveri, G.; Gottardi, G.; Hannan, M.A.; Anselmi, N.; Poli, L. Autocorrelation-driven synthesis of antenna arrays—The case of DS-based planar isophoric thinned arrays. *IEEE Trans. Antennas Propag.* **2019**, *68*, 2895–2910. [CrossRef]

32. Chang, B.K.; Ma, X.; Sequeira, H. Minimax-maxmini algorithm: A new approach to optimization of the thinned antenna arrays. In Proceedings of the IEEE Antennas and Propagation Society International Symposium and URSI National Radio Science Meeting, Seattle, WA, USA, 20–24 June 1994; IEEE: Piscataway, NK, USA, 1994; Volume 1, pp. 514–517.

33. Keizer, W.P. Amplitude-only low sidelobe synthesis for large thinned circular array antennas. *IEEE Trans. Antennas Propag.* **2011**, *60*, 1157–1161. [CrossRef]

34. Liu, Y.; Zheng, J.; Li, M.; Luo, Q.; Rui, Y.; Guo, Y.J. Synthesizing beam-scannable thinned massive antenna array utilizing modified iterative FFT for millimeter-wave communication. *IEEE Antennas Wirel. Propag. Lett.* **2020**, *19*, 1983–1987. [CrossRef]

35. Chen, J.; Yin, Y. Novel thinning computation approach for phased only rectangular array pattern synthesis. *IEICE Electron. Express* **2024**, *21*, 20240157. [CrossRef]

36. Tumolo, R.M.; D'Urso, M.; Prisco, G.; Buonanno, A. Fast synthesis of planar, maximally thinned arrays. *Prog. Electromagn. Res. Lett.* **2017**, *68*, 47–52. [CrossRef]

37. El-Khamy, S.E.; Eltrass, A.S.; El-Sayed, H.F. Adaptive beamforming synthesis for thinned fractal antenna arrays. In Proceedings of the 2017 XXXIInd General Assembly and Scientific Symposium of the International Union of Radio Science (URSI GASS), Montreal, QC, Canada, 19–26 August 2017; IEEE: Piscataway, NK, USA, 2017; pp. 1–4.

38. Rocca, P.; Anselmi, N.; Oliveri, G.; Polo, A.; Massa, A. Antenna array thinning through quantum Fourier transform. *IEEE Access* **2021**, *9*, 124313–124323. [CrossRef]

39. Bae, J.H.; Kim, K.T.; Pyo, C.S.; Chae, J.S. Design of Scannable Non-uniform Planar Array Structure for Maximum Side-Lobe Reduction. *ETRI J.* **2004**, *26*, 53–56. [CrossRef]

40. Donelli, M.; Caorsi, S.; De Natale, F.; Franceschini, D.; Massa, A. A versatile enhanced genetic algorithm for planar array design. *J. Electromagn. Waves Appl.* **2004**, *18*, 1533–1548. [CrossRef]

41. Spence, T.; Werner, D. Thinning of aperiodic antenna arrays for low side-lobe levels and broadband operation using genetic algorithms. In Proceedings of the 2006 IEEE Antennas and Propagation Society International Symposium, Albuquerque, NM, USA, 9–14 July 2006; IEEE: Piscataway, NK, USA, 2006; pp. 2059–2062.

42. Jain, R.; Mani, G. Solving "Antenna Array Thinning Problem" Using Genetic Algorithm. *Appl. Comput. Intell. Soft Comput.* **2012**, *2012*, 946398. [CrossRef]

43. Gangwar, V.; Singh, A.; Thomas, E.; Singh, S. Side lobe level suppression in a thinned linear antenna array using particle swarm optimization. In Proceedings of the 2015 International Conference on Applied and Theoretical Computing and Communication Technology (iCATccT), Davangere, India, 29–31 October 2015; IEEE: Piscataway, NJ, USA, 2015; pp. 787–790.

44. Cheng, Y.F.; Shao, W.; Zhang, S.J.; Li, Y.P. An improved multi-objective genetic algorithm for large planar array thinning. *IEEE Trans. Magn.* **2015**, *52*, 1–4. [CrossRef]

45. Ortiz, M.; Uddin, M.N.; Guerra, M.R.; Alwan, E.A. Enhancing Gain Through Optimal Antenna Element Distribution in a Thinned Array Configuration. *IEEE Open J. Antennas Propag.* **2023**, *4*, 1176–1186. [CrossRef]

46.  Gayatri, A.; Kumar, M.S.; Prasad, A. Multiobjective Optimization Using Modified Binary PSO for Reduction of Sidelobe Level of the Thinned Array Antenna. *Rev. Geintec-Gest. Inov. E Tecnol.* **2021**, *11*, 2715–2725. [CrossRef]

47.  Li, P.F.; Qu, S.W.; Yang, S.; Hu, J. Low-scattering-cross section thinned phased array antenna based on active cancellation technique. *IEEE Trans. Antennas Propag.* **2022**, *70*, 5481–5490. [CrossRef]

48.  Sun, Y.; Sun, J.; Ye, L. Synthesis of thinned planar concentric circular antenna arrays using a modified artificial bee colony algorithm. *Int. J. Antennas Propag.* **2023**, *2023*, 7735267. [CrossRef]

49.  Epcacan, E.; Ciloglu, T. A hybrid nonlinear method for array thinning. *IEEE Trans. Antennas Propag.* **2018**, *66*, 2318–2325. [CrossRef]

50.  Wang, L.; Wang, X.K.; Wang, G.; Jia, J.K. A two-step method for the low-sidelobe synthesis of uniform amplitude planar sparse arrays. *Prog. Electromagn. Res. M* **2019**, *86*, 153–162. [CrossRef]

51.  Qi, Z.; Bai, Y.; Zhang, X. Synthesis of linear and planar arrays via sequential convex optimizations. *IEEE Access* **2019**, *8*, 6717–6728. [CrossRef]

52.  Abdulqader, A.J.; Mahmood, A.N.; Mohammed Ali, Y.E. A Multi-Objective Array Pattern Optimization via Thinning Approach. *Prog. Electromagn. Res. C* **2022**, *127*, 251–261. [CrossRef]

53.  Lecci, M.; Testolina, P.; Rebato, M.; Testolin, A.; Zorzi, M. Machine learning-aided design of thinned antenna arrays for optimized network level performance. In Proceedings of the 2020 14th European Conference on Antennas and Propagation (EuCAP), Copenhagen, Denmark, 15–20 March 2020; IEEE: Piscataway, NK, USA, 2020; pp. 1–5.

54.  Jin, N.; Rahmat-Samii, Y. Advances in particle swarm optimization for antenna designs: Real-number, binary, single-objective and multiobjective implementations. *IEEE Trans. Antennas Propag.* **2007**, *55*, 556–567. [CrossRef]

55.  Petko, J.S.; Werner, D.H. Pareto optimization of thinned planar arrays with elliptical mainbeams and low sidelobe levels. *IEEE Trans. Antennas Propag.* **2011**, *59*, 1748–1751. [CrossRef]

56.  Pappula, L.; Ghosh, D. Sparse antenna array synthesis using multi-objective optimization. In Proceedings of the 2013 IEEE Applied Electromagnetics Conference (AEMC), Bhubaneswar, India, 18–20 December 2013; IEEE: Piscataway, NK, USA, 2013; pp. 1–2.

57.  Pappula, L.; Ghosh, D. Synthesis of thinned planar antenna array using multiobjective normal mutated binary cat swarm optimization. *Appl. Comput. Intell. Soft Comput.* **2016**, *2016*, 4102156. [CrossRef]

58.  Vankayalapati, S.; Pappula, L. Machine Learning Assisted Multi-Objective Planar Antenna Array Synthesis for Interference Mitigation in Next Generation Wireless Systems. *Prog. Electromagn. Res. M* **2023**, *119*, 129–142. [CrossRef]

59.  Vankayalapati, S.; Pappula, L.; Kumar, K.; Narayana Rao, K.; Raju, K.H.K.; Vinay, V.S. Approximating the pareto fronts for synthesis of planar antenna array using binary cat swarm optimization algorithm. *J. Phys. Conf. Ser.* **2023**, *2471*, 012023. [CrossRef]

60.  Hansen, R.C. *Phased Array Antennas*; John Wiley & Sons: Hoboken, NJ, USA, 2009.

61.  Mailloux, R.J. *Phased Array Antenna Handbook*; Artech House: Norwood, MA, USA, 2017 .

62.  Marler, R.T.; Arora, J.S. The weighted sum method for multi-objective optimization: New insights. *Struct. Multidiscip. Optim.* **2010**, *41*, 853–862. [CrossRef]

63.  Pinchera, D.; Perna, S.; Migliore, M.D. A lexicographic approach for multi-objective optimization in antenna array design. *Prog. Electromagn. Res. M* **2017**, *59*, 85–102. [CrossRef]

64.  Lai, L.; Fiaschi, L.; Cococcioni, M. Solving mixed Pareto-Lexicographic multi-objective optimization problems: The case of priority chains. *Swarm Evol. Comput.* **2020**, *55*, 100687. [CrossRef]

65.  Liang, J.; Ban, X.; Yu, K.; Qu, B.; Qiao, K.; Yue, C.; Chen, K.; Tan, K.C. A survey on evolutionary constrained multiobjective optimization. *IEEE Trans. Evol. Comput.* **2022**, *27*, 201–221. [CrossRef]

66.  Zitzler, E.; Thiele, L. Multiobjective evolutionary algorithms: A comparative case study and the strength Pareto approach. *IEEE Trans. Evol. Comput.* **1999**, *3*, 257–271. [CrossRef]

67.  Deb, K.; Pratap, A.; Agarwal, S.; Meyarivan, T. A fast and elitist multiobjective genetic algorithm: NSGA-II. *IEEE Trans. Evol. Comput.* **2002**, *6*, 182–197. [CrossRef]

68.  Panduro, M.A.; Covarrubias, D.H.; Brizuela, C.A.; Marante, F.R. A multi-objective approach in the linear antenna array design. *AEU-Int. J. Electron. Commun.* **2005**, *59*, 205–212. [CrossRef]

69.  Pinchera, D. On the trade-off between the main parameters of planar antenna arrays. *Electronics* **2020**, *9*, 739. [CrossRef]

70.  Bai, Y.Y.; Xiao, S.; Tang, M.C.; Ding, Z.F.; Wang, B.Z. Wide-angle scanning phased array with pattern reconfigurable elements. *IEEE Trans. Antennas Propag.* **2011**, *59*, 4071–4076.

71.  Pinchera, D.; Lucido, M.; Chirico, G.; Schettino, F.; Migliore, M.D. Controllable local propagation environment to maximize the multiplexing capability of massive MIMO systems. *Electronics* **2023**, *12*, 2022. [CrossRef]

72.  Meng, C.; Zhang, Y.; Temiz, M.; El-Makadema, A. A Multiobjective Array Beamforming Method for Arrays of Flexible Shape. *Electronics* **2024**, *13*, 752. [CrossRef]